Wireless Electrical-Molecular Quantum Signalling for Cancer Cell Induced Death

Akhil Jain,[1] Jonathan Gosling,[2] Shaochuang Liu,[3] Haowei Wang,[3] Eloise M. Stone,[4] Lluïsa Pérez-García,[5,6] David B. Amabilino,[7] Mark Fromhold,[8] Stuart Smith,[9,10] Ruman Rahman,[9] Yitao Long,[3] Lyudmila Turyanska,[2] Frankie J. Rawson[1,*]

[1]*Bioelectronics Laboratory, Division of Regenerative Medicine and Cellular Therapies, School of Pharmacy, University of Nottingham, Nottingham, NG7 2RD, UK*

[2]*Faculty of Engineering, University of Nottingham, Nottingham, NG7 2RD, UK*

[3]*State Key Laboratory of Analytical Chemistry for Life Science, School of Chemistry and Chemical Engineering, Nanjing University, Nanjing 210023, China*

[4]*School of Pharmacy, University of Nottingham, Nottingham, NG7 2RD, UK*

[5]*Department of Pharmacology, Toxicology, and Therapeutic Chemistry, Faculty of Pharmacy and Food Science, University of Barcelona, 08028 Barcelona, Spain.*

[6]*Institute of Nanoscience and Nanotechnology, University of Barcelona (IN2UB), 08028 Barcelona, Spain*

[7]*Institut de Ciència de Materials de Barcelona (ICMAB-CSIC), Campus Universitari de Cerdanyola, 08193 Spain*

[8]*School of Physics and Astronomy, University of Nottingham, University Park, Nottingham, NG7 2RD, UK*

[9]*Children's Brain Tumour Research Centre, School of Medicine, University of Nottingham, Biodiscovery Institute, Nottingham, NG7 2UH, UK*

[10]*Department of Neurosurgery, Nottingham University Hospitals, Nottingham, NG7 2UH, UK*

*****Corresponding author: Frankie.Rawson@nottingham.ac.uk

Word Count (excluding figure legends and references) = 3402.

Word Count (excluding references) = 4502. Word limit = 3000 - 4500 words

Abstract (Word Count: 149)

Quantum biological electron tunnelling (QBET) underpins cellular behaviour. Control of electrical-molecular communication could revolutionise the development of disruptive technologies for understanding and modulating molecular signalling. Current communication technology is not appropriate for interfacing with cells at a spatial/temporal level equivalent to the native biological signalling. We merge bipolar nano-electrochemical tools with cancer cells. Gold-bipolar nanoelectrodes functionalised with electron acceptor-donor-species, were developed as electric field bio-actuators we term bio-nanoantennae. Remote electrical input regulated electron transport between the acceptor-donor species at the bio-nanoantennae in a selective manner. The wireless modulation of electron transport results in QBET triggering apoptosis in patient-derived cancer cells representing electrical-molecular communication. Transcriptomics data highlight the electric field targets the cancer cells in a unique manner. The stated insight and invention open a plethora of applications in healthcare. This may lead to new quantum-based medical diagnostics and treatments, as well as understanding of the biological physics.

Keywords: electron transfer; wireless electrochemistry; bipolar nanoelectrodes, electric fields; differential gene expression; glioblastoma; gold nanoparticles; cytochrome *c* and zinc porphyrin.

Word Count = 671

Cells modulate their function through the control of electrical currents and are essential to life. There is now evidence indicating that we are entering a new era, where bioelectricity, defined as the electrical language of cells, is a key dogma in biology.[1,2] The cell is increasingly viewed as a mass of bioelectrical interconnected circuits.[3] One of the most well-known electron transfer pathways is photosynthesis and was one of the first whose mechanism was linked to quantum mechanical effects.[4,5] Quantum biology is still in its infancy, future developments in biology and medicine are expected to be underpinned by understanding of quantum mechanical

processes.[6] Cytochrome *c* (Cyt *c)* can induce apoptosis when its redox state is modulated through an electron transfer process at the heame.[7] This can occur via electron tunnelling.[8,9,10] However, our ability to electrically communicate with such systems is limited by a mismatch in communication technology and selective targeting bio-interfacing of electrical actuation systems.

Electrical-molecular communication inside cells opens the possibility of creating new disruptive technologies, including the development of new quantum medicines for cancer treatments.[11] However, on-demand targeted electrical-molecular communication within cells are yet to be realised, mostly due to lack of suitable communication technologies for interfacing with cells at a spatial/temporal level observed in native biological communication that occurs. Moreover, technological innovation in electrical transduction via bio-nanoantenna (defined as receiving an electrical input and converting to biological output) capable of receiving externally applied electrical input and converting this to bio-signalling events has not been achieved. The aim of this study was therefore to pioneer solutions to these problems.

Gold nanoparticles[12] and carbon nanotubes have recently been shown can act as bipolar nanoelectrodes[13] within cells when external electric fields (EFs) are applied. The bipolar nanoelectrodes become polarised when an EF is applied, leading to a voltage gradient across the particle. With sufficiently large potential difference at the poles, the thermodynamic driving force can cause electrochemically-induced redox reactions to occur.[14,15] It was thought that nanoscale bipolar electrochemistry was not possible in the presence of cells even at high applied voltages.[16,17] Importantly, most recently bipolar electrodes in series lead to a dramatic drop in cell impedance,[18] which may allow electrical inputs to be used without inducing cell damage. Redox reactions at carbon nanotube porins, acting as bipolar nanoelectrodes, can occur at unprecedented applied low voltages with cells without inducing direct cell death.[19]

We, therefore, hypothesised an approach that uses bi-functionalised bipolar nanoelectrodes with an acceptor-donor-species attached, we term bio-nanoantennae, in combination with applied EFs could be used to modulate electron transfer. This electronic signal is then converted into a molecular actuation in a specific targeted metabolic pathway (Fig. **1**).

The strategy to fulfil the development of the first quantum electrical-molecular communication tool was multi-pronged. Firstly, we were inspired by the observation that cyt *c* electron transfer is mediated through quantum biological electron tunnelling (QBET).[10] Therefore, we functionalised gold nanoparticles (GNPs) with electron donor cyt *c* and redox acceptor in the form of zinc porphyrin (Z) with the conductive nanoparticle forming an electronic bio-nanoantenna (Fig **1a**). We show that on the application of an external electric field wireless electrochemistry is induced at the nanoparticle surface switching the oxidation state of cyt *c*. We show that the electrical input confers specific signalling to cells via the bio-nanoantennae to induce GBM cell death through apoptosis (Fig **1b**). We used multiple analytical approaches to show the redox state of the cyt *c* changes with a resonant electrical input of alternating current electric field (AC-EF) at 3 MHz using an applied voltage of 0.65V/cm. We propose that QBET phenomenon and resonant electron transfer between the cyt *c* and Z to facilitate cellular apoptosis (Fig **1c**). The transcriptomic analysis enabled elucidation of the biochemical signalling when using the quantum electrical-molecular communication tool (Fig **1d**). The data suggest that electrical field molecular actuation is disease targeting, which may represent a first-in-class quantum functional medicine tool (Fig **1e**) and could open exciting opportunities for development of quantum nanomedicines and cancer treatments and provide a new means of modulating cell metabolism.

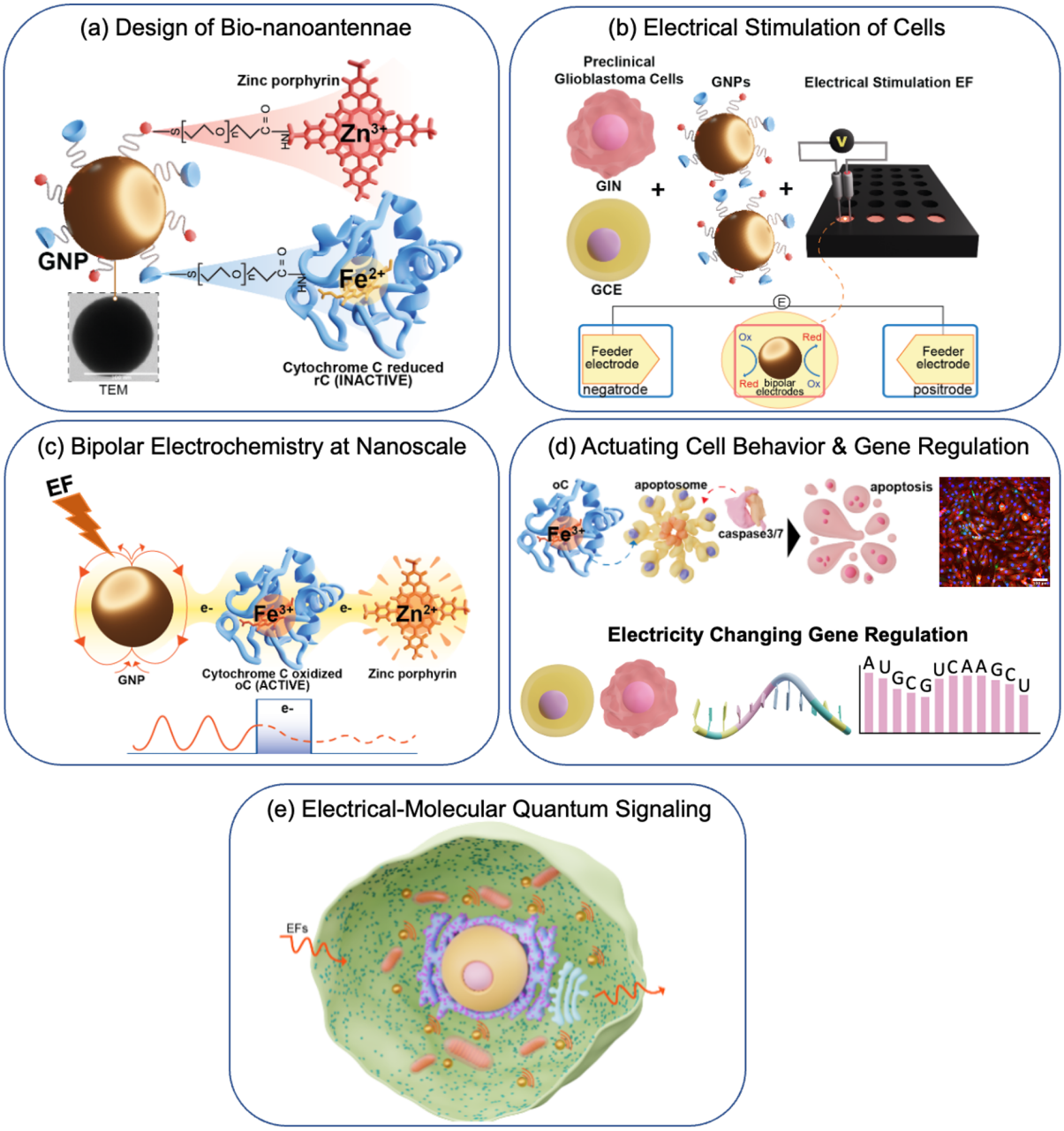

Figure 1. Schematic illustration of AC-EF responsive bio-nanoantennae mediated wireless electrical-molecular quantum signalling to induce cell death. (a) Bio-nanoantennae were synthesised by covalently conjugating reduced form of Cyt *c* (rC) and Zinc Porphyrin (Z) to carboxylic PEG functionalised 100 nm citrate capped gold nanoparticles (GNP.100) using EDC/NHS chemistry. **(b)** These synthesised bio-nanoantennae (GNP100@rC@Z) were incubated with primary patient-derived GBM cells viz. GIN (derived from the GBM infiltrative margin) and GCE (derived from the GBM proliferative core) cells

to enable their uptake. These GBM cells are electrically stimulated (ES) with AC EFs of 3 MHz at 0.65 V/cm. **(c)** AC EFs were applied to induce bipolar electrochemistry at the surface of bio-nanoantennae intracellularly to switch the redox state of cyt c (reduced to oxidised) and Z. **(d)** These applied AC EF caused the intracellular bipolar electrochemistry to occur at bio-nanoantennae surface thus inducing caspase 3/7 mediated apoptosis of GBM cells. Understanding the electrical-molecular signalling by connecting gene regulation with AC EFs mediated cell death in GBM cells. **(e)** Diagrammatic representation to demonstrate AC EFs responsive bio-nanoantennae for Electrical-Molecular Quantum Signalling with GBM cells.

Design of bio-nanoantennae for actuating cancer cell death *(WC: 875)*

To electrically communicate with biology at an equivalent level to that underpinning molecular biochemistry, we initially used 100 nm PEGylated spherical gold nanoparticles (GNP100) as bipolar nanoelectrodes that can be functionalised to yield nanoantennae for biology. These GNPs can sense electric field applied extracellularly and drive surface redox reactions,[12,18] which could modulate the redox state of surface-bound Z and cyt *c* that would actuate a cell-specific signalling pathway, apoptosis. Apoptosis is in part mediated by cyt *c* bioelectrochemistry in which its oxidised state (Fe^{3+}) facilitates apoptosis-mediated cell death.[20] Therefore, we functionalised GNP100 with an electrical donor reduced (inactive; Fe^{2+}) cyt *c* (rC) and oxidised receptor Z through carbodiimide coupling chemistry to form bio-nanoantennae (GNP100@rC@Z) (Figure 1a, Supplementary Information, SI1). On application of an electric field the particles would polarise providing the thermodynamic driving force to oxidize the rC and reduce the Z .[21] To validate our hypothesis and QBET, the effect of the NP size and the PEG linker length, 20 and 50 nm particles were also functionalised with rC and Z using PEG linker of varying length (1 KDa, 2 KDa, 3.5KDa, 5 kDa) to yield different size bio-nanoantennae (GNP20@rC@Z and GNP50@rC@Z).

The successful bifunctionalisation of PEGylated (2 kDa) 100 nm citrate capped GNPs (GNP100) with rC and Z, is evident from the size of GNP100@rC@Z. The diameter of (GNP100@rC@Z) as analysed by TEM was found to be around 105 ± 2 nm (Fig. **2a i & ii**). The Dynamic Light Scattering (DLS) analysis that the average hydrodynamic diameter (h_d) increased from 104.9 nm (PEGylated GNPs) to 118.8 nm for the GNP100@rC@Z, suggesting successful conjugation of rC and Z (Supplementary Fig. **1**). A change in zeta potential (ζ) of GNP100@rC@Z (-28.5 mV) compared to GNP100 (-27.7 mV), GNP100@rC (-14.8 mV), and GNP100@Z (-40 mV) suggested the bi-functionalisation process was successful (Supplementary Fig. **2**). In addition, there was no significant change in h_d and ζ after electrical stimulation (ES) with AC electric fields (AC EF) of 3 MHz at 0.65V/cm suggesting the surface chemistry of the synthesised nanoantennae was stable. UV-Vis absorption spectrum of GNP100@rC@Z before ES in PBS revealed a broad peak centred at 418 nm attributed to overlapping absorption of rC and Z (Fig. **2 b & c**). This peak was deconvoluted and Marquardt fitting algorithm was applied,[22] which revealed two components centred at 412 nm and 423 nm attributed to rC and Z (Supplementary Fig. **3a & b**), respectively, which were corroborated using UV-Vis spectrum of native rC and Z in PBS (Supplementary Fig. **S3c**). The obtained peaks were used for the quantification of rC, and Z attached to each GNP100@rC@Z, which revealed homogenous and monolayer conjugation of rC and Z on GNP100 (Supplementary Fig. **3d-e** and Table **1-4**). Cyclic voltammetry was carried out to study the redox behaviour of rC and Z on a bifunctionalised system (Fig. **2d**). Two redox couples were observed in GNP100@rC@Z, which are attributed to cyt *c* and Z, while on the other hand, the control samples only showed a redox couple corresponding to either cyt *c* or Z, which have been characterised by others previously (Supplementary Fig. **4 a-c**).[23,24] The heterogenous electron transfer rate coefficient (k^0) of cyt *c* for GNP100@rC@Z (Supplementary Fig. **5a-f**) was calculated to be 3.75 × 10^{-3} cm/s, while that for GNP100@rC was 9.6 × 10^{-3} cm/s

(Supplementary Table **5**), suggesting a slight increase in electron transfer rate of cyt *c* in a bifunctionalised system.

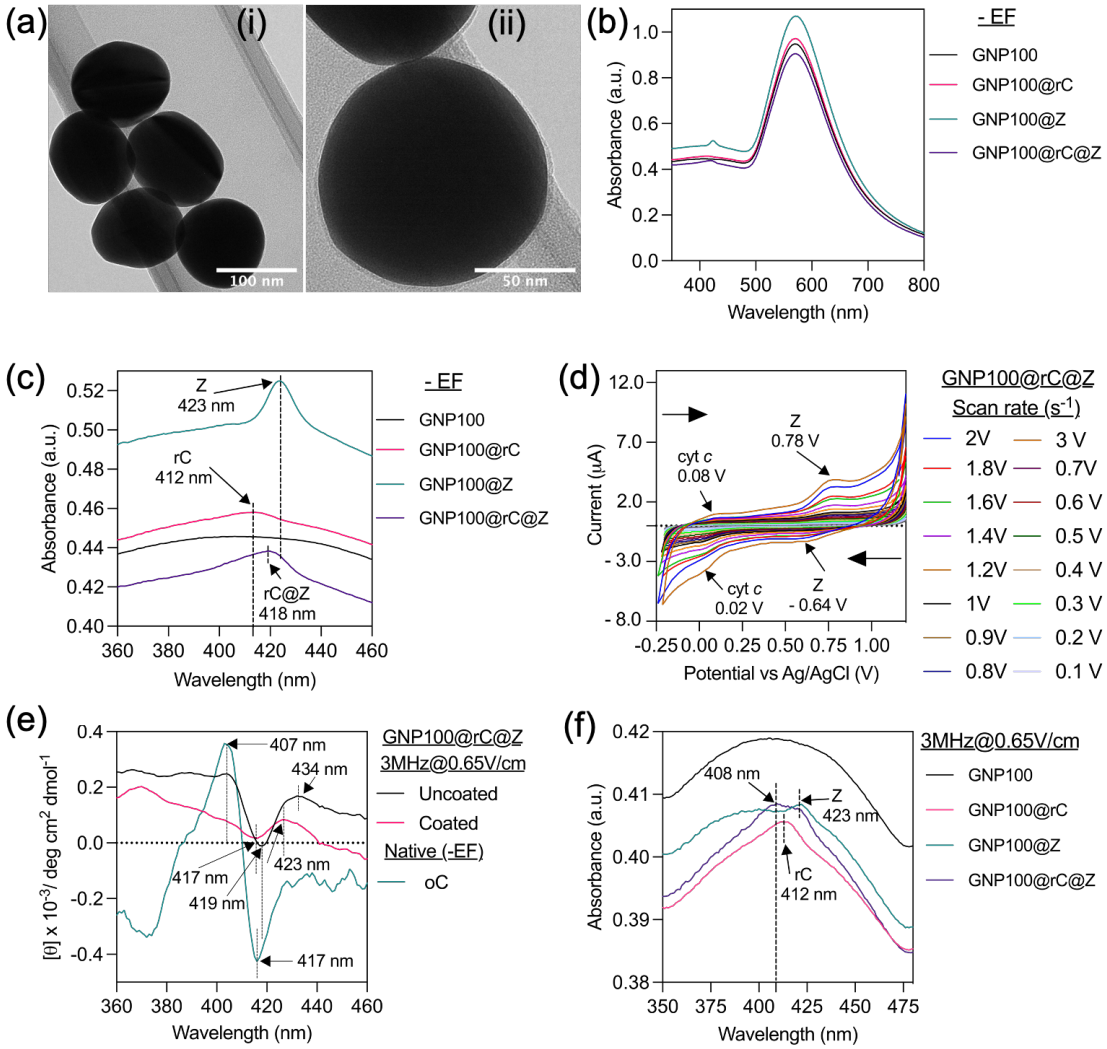

Figure 2. Designing AC-EFs responsive bio-nanoantennae for wireless electrical-molecular communication with cells via redox switching of cyt *c*. (a - i & ii) Transmission electron microscopy (TEM) of bio-nanoantennae (GNP100@rC@Z) prepared by coupling reduced cyt *c* (rC) and Zinc porphyrin (Z) to 100 nm PEGylated gold nanoparticles (GNP100). **(b)** UV-Vis absorption spectrum of bio-nanoantennae dispersed in PBS before ES. **(c)** High resolution UV-Vis spectrum to depict surface functionalisation with rC (GNP100@rC), Z (GNP100@Z), and both rC & Z (GNP100@rC@Z). **(d)** Cyclic voltammetry scan rate studies to analyse the redox properties of GNP100@rC@Z. Redox potentials measured using an

Indium tin oxide (ITO) working electrode, platinum wire counter and Ag/AgCl reference electrode with samples (25 µg/mL) dispersed in 10 mM PBS. **(e)** The effect of AC-EFs on the conformation of redox moieties**:** high resolution of soret CD spectrum to emphasise redox mediated change in haem moieties of free native oC, rC, and bifunctionalized GNP nanoactuators in 10 mM PBS (pH = 7.4). All samples with identical concentration (25 µg/mL) were used for spectrum acquisition. Three spectra of each sample were collected and averaged. Insulated coated steel electrodes were used as a control to demonstrate the occurrence of nanoscale BPE. **(f)** High resolution UV-Vis spectrum of bi-nanoantennae after stimulation with AC-EFs of 3MHz, 0.65V/cm indicating blue shift in absorption maxima of rC to oC (oxidised cyt *c*) in GNP100.@rC@Z

The electrical-molecular communication via bipolar electrochemistry induced at GNP100@rC@Z, was probed by circular dichroism (CD) analysis (Fig. **2e** and Supplementary Fig. **6 a-e**). The soret CD spectrum of GNP100@rC@Z revealed two positive maxima (407 nm and 434 nm) suggesting the oxidation of haem centre of cyt *c* and reduction of Z after ES with AC EFs of 3 MHz at 0.65 V/cm. This was corroborated by comparison with CD of native oC. Furthermore, one negative minimum (417 nm) was observed for native oC, which was red shifted to 419 nm indicating slight perturbation around the haem moiety. On the other hand, when a control experiment was carried out by performing ES of GNP100@rC@Z using insulated electrodes, we did not observe any signals from rC or oC, indicating significant perturbation of haem moiety. To further ascertain nanoscale BPE, the UV-Vis spectrum of GNP100@rC@Z was monitored after the ES (Fig. **2f** and Supplementary Fig. **7 a-c**), and revealed a significant blue shift in the absorbance peak of rC from 412 nm to 408 nm and red shift in the absorbance peak of Z from 423 nm to 432 nm, which can be attributed to the oxidation of the haem moieties in cyt *c* and reduction of the Z leading to the formation of J aggregates,[25] respectively. We note that no shift of absorption peaks was observed without EF

stimulation (Supplementary Fig. **8).** The obtained spectroscopic data confirms that we were successfully able to induce nanoscale BPE on the surface of GNP100@rC@Z to modulate the redox state of cyt *c* (Fe^{2+} to Fe^{3+}) using remotely controlled AC EFs. Thus, we demonstrate that the bio-nanoantennae act as bipolar electrodes and can modulate the REDOX state of the oC and Z under application of the EF. We envisage that these processes can be used to provide molecular communication with the cells to modulate their function.

AC EFs mediated intracellular BPE on bio-nanoantennae surface induces apoptosis in pre-clinical Glioblastoma (GBM) models *(Word Count: 835)*

To explore the potential of bio-nanoantennae, four types of preclinical GBM cells, isolated from two GBM patients: Glioma Invasive Margin (GIN 28 and GIN 31, isolated from infiltrative tumor), Glioma Contrast-Enhanced core (GCE 28 and GCE 31, isolated from central tumor), which echo similar characteristics to different regions of GBM tumours[26] and a commercial GBM cancer cell line U251 were selected. Human derived cortical astrocytes were also included as a control for non-tumorigenic cells. 3D analysis of z stacks confocal microscopy images **(**Supplementary Fig. **9)** and inductively coupled plasma – mass spectrometry (ICP-MS) (Supplementary Fig. **10**) confirmed that the particles were internalised by all cell lines used after 8 hours incubation. PrestoBlue assay data revealed that the particles are biocompatible up to a tested range of 100 µg/mL (Supplementary Fig. **11**). The voltage and frequency were optimised (Supplementary Fig. **12**) by assessing change in metabolic activity of GIN 31 cells using PrestoBlue assay. The maximum effect on cell viability was observed at 3 MHz, at an applied potential of 1V/cm and 0.65V/cm (no significant difference between 0.65 V/cm *vs* 1V/cm, p value = 0.23) with significant differences between the tested controls (GNP100, GNP100@rC, and GNP100@Z) and the bifunctionalised bio-nanoantennae (GNP100@rC@Z). Importantly, the observed decrease of metabolic activity of GNP100@rC@Z treated cells was significantly higher than that following 24-hour application

of FDA approved Tumour treating Fields (TTFs) *in vitro*.[27,28] We ascribe this significant decrease in metabolic activity to the electrical-molecular communication via redox switching of rC to oC, thus inducing cells stress. To eliminate any potential effect of applied 1V on water electrolysis (1.23 V *vs* normal hydrogen electrode), we chose 0.65 V/cm for further studies. The response of the cells to the treatment with GNP100@rC@Z bio-nanoantennae was comparable in different patient derived GIN and GCE cells (Fig. **3 a & b**), with a significant ~ 50% decrease in metabolic activity achieved after 12 h *vs* a ~ 20% decrease after 2 h AC EF stimulation (Supplementary Fig. **13**). This decrease in metabolic activity was significantly higher compared to the control (*p* values obtained from the statistical analysis are listed in supplementary table **6**). On the other hand, a significantly weaker effect (~ 20% decrease in metabolic activity) was observed in cortical astrocytes, which was found to be not significantly different from the control (Fig. **3c**). Thus, based on the obtained data, we draw a conclusion that the change in metabolic activity depend on the duration of treatment and cell type.

The alteration in metabolic activity in cells treated with GNP100@rC@Z + AC EFs (3 MHz at 0.65 V/cm for 12 hours) is correlated with increased cell death, as clearly evidenced by the results of live-dead assay (Supplementary Figs. **14 & 15**). The mechanism of cell death was probed by flow cytometry (Fig. 3 d-g and Supplementary Figs. 16 & 17) and confocal microscopy (Fig. 3h and Supplementary Fig. 18), where the induced caspase 3/7 activity was observed in GIN/GCE cells treated with GNP@rC@Z followed by ES, indicative of apoptosis.[29] The confocal microscopy revealed that bio-nanoantennae are localised within the cytosol (Fig. **3i**). We note that no reactive oxygen species and temperature changes were observed (Supplementary Figs. **19 & 20**). Therefore, we successfully conducted ES of GBM cells and demonstrated bipolar electrochemistry mediated redox switching and activation of cyt *c* on the surface of GNP100@rC@Z leading to apoptosis of GBM cells.

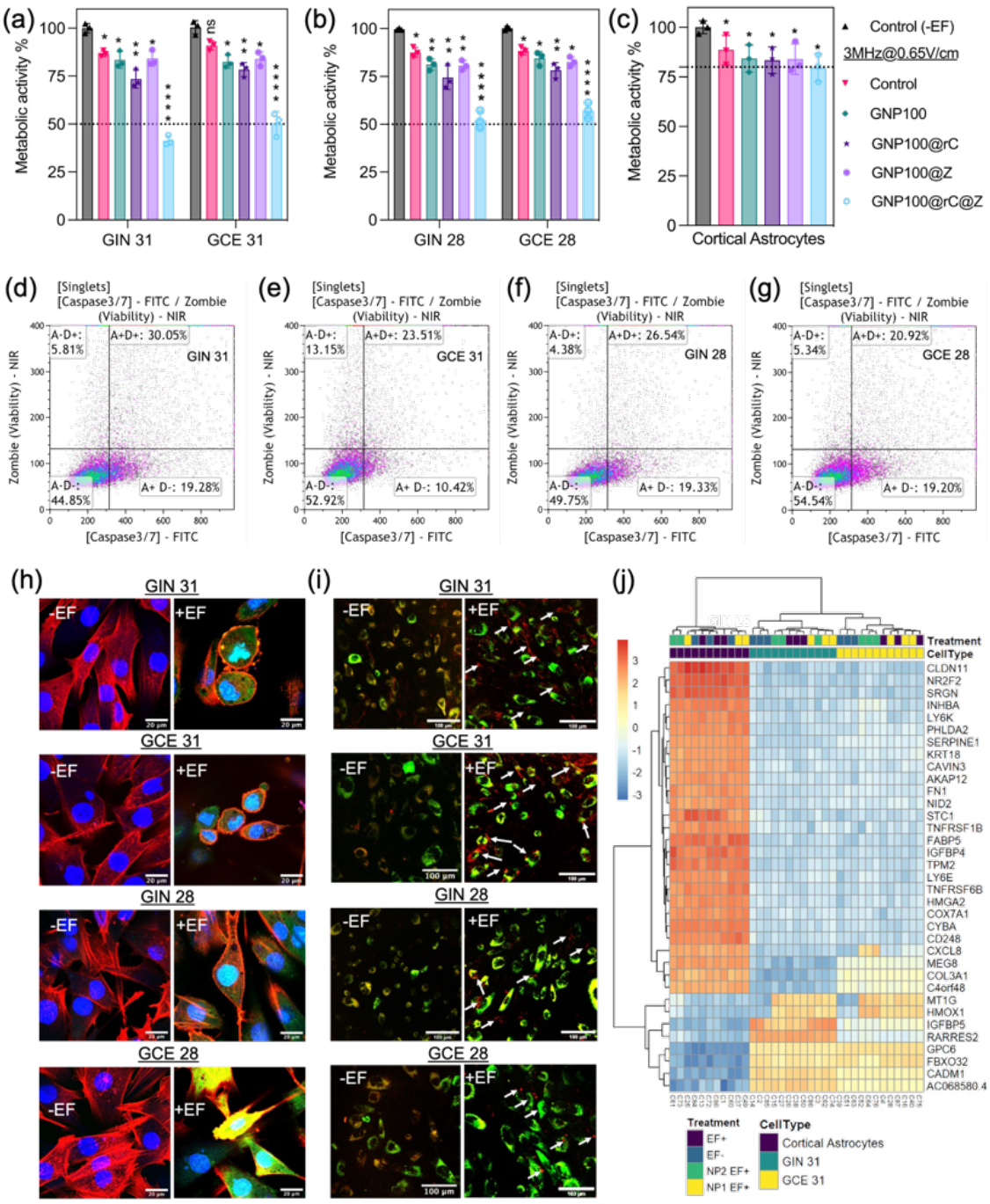

Figure 3. AC-EF responsive bio-nanoantennae mediated wireless electrical molecular communication to induce caspase 3/7 mediated apoptosis in preclinical glioblastoma cells. **(a-c)** Metabolic activity of GIN/GCE 31, GIN/GCE 28, and cortical astrocytes was analysed using PrestoBlue HS assay. GIN, GCE, human cortical astrocytes were treated with GNP100@rC@Z for 8 h followed by AC-EFs stimulation (3MHz, 0.65V/cm) for 12 h. Error bars represent mean ± standard error of mean (S.E.M.) obtained from triplicate experiments

repeated thrice. Statistical analysis was performed by applying 2-way ANOVA with a Tukey's post-test **(d-g)** Representative samples of flow cytometric analysis of cells stained with CellEvent Caspase-3/7 Green to detect caspase 3/7 apoptotic activity and Zombie NIR fixable dye to detect dead cell population. The quadrants in the figure represents the following: A+ = caspase 3/7 positive apoptotic cells and D+ = non-viable/dead cells. **(h)** High-magnification confocal microscopy images to demonstrate caspase 3/7 activation immediately after the treatment with AC-EFs (3MHz, 0.65V/cm) for 12 h in presence of bio-nanoantennae. Cells were fixed with paraformaldehyde followed by counterstaining with caspase 3/7 green detection kit, Cytopainter actin phalloidin (Texas Red 591 red), and Hoechst nuclear stain (blue). Scale bar = 20 mm. **(i)** Confocal microscopy image to demonstrate cytoplasmic localisation of GNP100@rC@Z immediately after the treatment with AC-EFs (3MHz, 0.65V/cm) for 12 h in presence of bio-nanoantennae. Cells were stained with late endosome dye (green) and imaged using a Leica confocal microscope with GFP (late endosomes) and Alexa 633 (GNP100@rC@Z) filter settings. Scale bar = 100 mm. **(j)** Heat map demonstrating hierarchical clustering of top 35 genes that were regulated after the treatment with GNP100@rC@Z for 8 h followed by AC-EFs stimulation (3MHz, 0.65V/cm) for 2-hour. A variance stabilised transformation was performed on the raw count matrix and 35 genes with the highest variance across samples were selected for hierarchical clustering. Each row represents one gene, and each column represents one sample. The colour represents the difference of the count value to the row mean. GIN/GCE 31 which showed maximum response to the treatment with GNP100@rC@Z and AC EFs were chosen. As a control to cancer cells, healthy cortical astrocytes were used. Immediately after the treatment, cells were washed and centrifuges to obtain a pellet, which was snap frozen in liquid nitrogen and shipped (in dry ice) to Qiagen, Ltd, Germany for RNA sequencing. The treatment codes in Fig. 1j are as follow: - EF = Control (no treatment with either bio-nanoantennae or AC EFs); + EF = cells treated with

AC EFs; NP1 EF+ = cell treated with GNP100@rC, and NP2 EF+ = cells treated with GNP100@rC@Z, for 8 h followed by 2-hour AC EFs.

To further understand this electrical-molecular signalling. We performed transcriptomic analysis on a sample of glioblastoma cells and astrocytes (Fig **3j** and Supplementary Figs **S21-22)** to interrogate the effect of the bioelectronic communication tool on gene expression and regulation. Hierarchical clustering analysis showed differential expression of genes related to apoptosis, cancer proliferation and angiogenesis, and tumour suppression. This change in differentially expressed genes was highest for GIN/GCE 31 cells treated with GNP100@rC@Z followed by ES compared to untreated cells and other experimental controls. Gene ontology analysis revealed that most of the differentially upregulated genes such as CXCL8 & INHBA in GCE 31, and MT1G & HMOX1 in GIN/GCE 31 are related with apoptosis, implying that apoptosis was upregulated after the treatment.[30-33] Furthermore, the upregulation of HMOX1 (a haem oxygenase) could also be due to the presence of haem containing cyt *c* and Z on bio-nanoantennae. On the other hand, most of downregulated genes such as STC1 (GIN 31), IGFBP5 (GIN/GCE 31), and FBXO32 (GIN/GCE 31) are characteristic of angiogenesis in cancer proliferation, and tumour growth and metastasis, respectively.[34-37] Interestingly, we didn't observed any changes in the gene regulation for astrocytes, this suggest that the treatment modulate signalling pathways that are specific only to GBM. Further studies are required to understand biological processes that are implicated during this treatment, which however are outside the scope of this work. Altogether the obtained data implies that GNP100@rC@Z treatment followed by ES leads to an increase in apoptosis, and reduced proliferation and invasiveness of patient derived GBM cells. Overall, the *in vitro* results indicate successful communication with biology at a molecular scale using electricity. Importantly, this approach enables selective actuation of cancer cell behaviour (diseased *vs* healthy cells) compared to astrocytes.

In vitro QBET *(Word count: 738)*

To facilitate the translation of the technology more broadly, understanding of the electrically induced mode of electron transfer is needed. The frequency we used for electrical communication was 3 MHz Considering the electron transfer rate constant of 3.75×10^{-3} cm/s calculated from Fig **2d**, the maximum distance the electron could travel at this frequency is 0.01 nm. Thus, theoretically at this given frequency, the redox event should not occur. We propose that the observed activity is enabled by quantum biological electron tunnelling (QBET) induced from the *cyt c* as was indicated previously.[10] However this has never been controlled through electrical stimulation.

To gather experimental evidence for QBET in our system, we consider molecular tunnel junctions (MTJs), where quantum electron tunnelling can occur.[38-41] Therefore, we altered the tunnel junction energy by using GNP with different sizes (20, 50, and 100 nm), and PEG linker with different length (1, 2, 3.5 and 5k Da) (Supplementary Figs. **S23 & 24**). The metabolic assays (Fig **4 a-c** & Supplementary Figs. **25 & 26**) and viability studies (Supplementary Figs. **27 & 28**) on GIN 31 cells with ES (3 MHz and 0.65V/cm) indicated a resonant biological effect with bifunctionalised bio-nanoantenna using the 1 kDa PEG linker with 50 nm and 100 nm GNPs. Importantly, this effect is only seen for cells treated with bio-nanoantennae (GNP@rC@Z) following 12 h ES. ICP-MS analysis revealed no significant different in the number of Z/rC per cells when treated with GNP20@rC@Z/ GNP50@rC@Z/ GNP100@rC/z (Supplementary Figs. **S29 & 30**). The explanation for this is garnered from the work of Hongbao Xin et al. which showed that the QBET could be captured from *cyt c* by tuning the tunnel junction via size of SAM linker.[10] We envisage that similar phenomenon in occurring in our system, as evidenced by the resonance at specific conditions and is indicative of wave-like behaviour.[42] Thus, we tentatively suggest that the electron transfer is a QBET, and this is

the first example of an electrically stimulated QBET in biology to date. Thereby facilitating electrical-molecular communication.

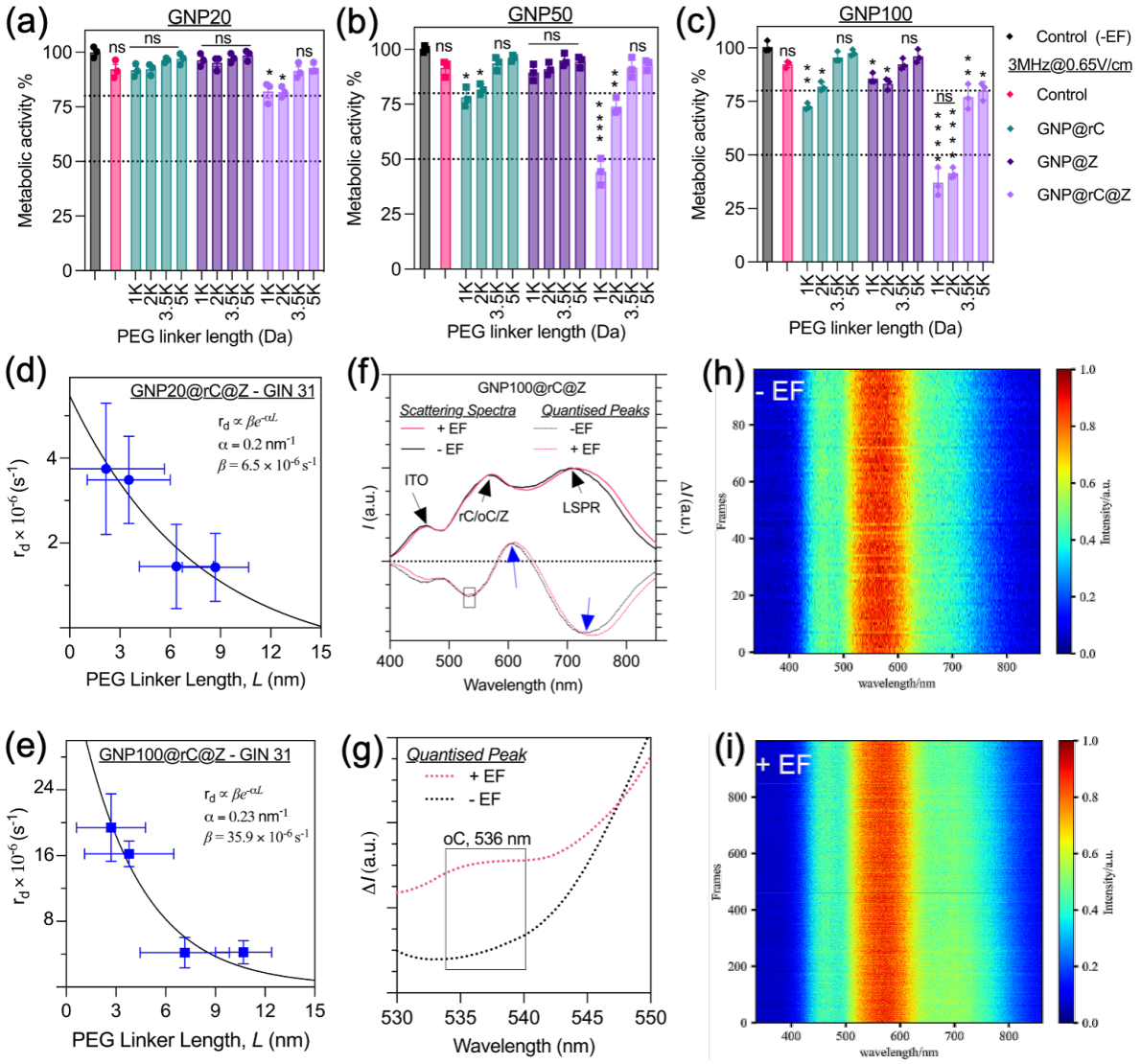

Figure 4. Wireless electrical-molecular quantum signalling: *in vitro* electron tunnelling via bio-nanoantennae for inducing cell death in GBM cells. (a-c) Metabolic activity of GIN 31 cells as function of different size (20 nm, 50 nm, and 100 nm) bio-nanoantennae (GNP20@rC@Z, GNP50@rC@Z, and GNP100@rC@Z) synthesised using various linker lengths (1k, 2k, 3.5k, and 5k Da). GIN 31 cells were treated with bifunctionalised bio-nanoantennae for 8 h followed by AC-EFs stimulation (3 MHz, 0.65V/cm) for 12 h. **(d-e)** Rate of donor charging, r_d, calculated using the metabolic activity, using equation no. 1, compared

to the PEG linker length, L, for (d) GNP100@rC@Z and (e) GNP20@rC@Z in GIN31 cell samples. The black lines show the exponential behaviour expected for quantum tunnelling with an inverse localisation radius α and constant of proportionality β shown in the figure legends. **(f)** Scattering spectra and spectra difference for QBET obtained for GNP100@rC@Z bio-nanoantennae. The quantised peaks were obtained from the difference of scattering spectra between the samples functionalised with rC and Z using 2000 Da linker and GNP100. Solid curves are captured scattering spectra (linked to left axis) of GNP100@rC@Z, and dashed curves are quantised peaks i.e., the corresponding spectra difference (linked to right axis). Blue boxes indicate peak shift. **(g)** High-resolution quantised peaks of region 530-550 nm in GNP100@rC@Z confirming the presence of oC in samples exposed to AC EFs. **(h-i)** Two-dimensional heat map of scattering spectral changes obtained from dark field microscopy, in the presence and absence of EF.

To provide further evidence of the mechanism of electron transfer we establish a mathematical model. The cell metabolic rate (Fig. 4a) was correlated to the rate of charge transfer from the cyt c derived equation no. 1 (full details of the derivation can be observed in Supplementary information section 1.6. of materials and methods). These values were then plotted as a function of the barrier junction altered using the ligand for different sized nanoparticles (Fig. **4 d-e**).

$$r_d = -\frac{\ln(M(t))}{t} \qquad \text{Eq (1)}$$

where r_d is rate of donor charging and $M(t)$ is metabolic activity at time t .

The results are well fitted with exponential dependences expected for the tunnelling of an electron through a barrier.[43] Supporting the fact that the resonance biological effects are observed with the electrical input results in a QBET. Further primary experimental evidence for the quantum tunnelling is provided by the plasmon resonance scattering spectroscopy (PRS) probing plasmon resonance energy transfer (PRET).[44] Scattering spectra were obtained for

GNP100@rC@Z with and without ES. Without ES, quantised dips were obtained by subtracting the spectra for the unmodified particle and vice-versa. For GNP100@rC@Z samples (no ES) the scattering peaks were observed at ~ 465 nm corresponding to ITO, a broad peak due to rC and Z at around 568 nm and localised surface plasmon resonance (LSPR) peak shifted to 711 nm (GNP100 sample LSPR = 612 nm) (Fig. **4f** and Supplementary Fig **31a**). This equates to the frequencies with the absorption peak of rC/Z and subsequently induces the electronic excitation of the rC at the specific wavelength.[10] Importantly, the QBETs captured are cumulative. Under ES, we see a quantised dip at 536 nm due to the switching of rC to oC and thus representing QBET (Fig. **4g**). We also see a 20 mV shift in the SPR peak (heat maps Fig. **4h**: no EF, and Fig. **4i**: EF applied) indicative of charge transfer, which we tentatively associate with the acceptor donor complex redox behaviour.[45,46] It is important to note that the appearance of oC was not observed in all other control samples with ES (3MHz, 0.65V) (Supplementary Fig **31 b-i**). The data combined indicated resonant frequency resulting in cell death, model exponential decay based on barrier junction energetics and PRET data resulting in quantised dips that represent electron tunnelling. Therefore, we tentatively suggest that this is the first successful demonstration of electrical-molecular quantum signalling technology in biology, which we demonstrated could be used for cancer killing.

3. Conclusions (Word count: 134)

To summarise our findings. We have designed, a bio-nanoantennae system inspired by bipolar electrochemistry that is sensitive to electric fields. These were based on gold nanoparticles functionalised with an electron acceptor-donor species. On application of electric fields, the redox state of molecules functionalised on the surface of nanoantennae could be tuned. Bio-nanoantennae were then used to facilitate electrical-molecular communication with glioblastoma cells. This was demonstrated through the stimulation of specific cell response in the form of apoptosis. Achieved by modulating the redox state of the *cyt c*, which induces

apoptosis. We then infer that the electron transfer in the bio-nanoantennae may occur from electric field-induced quantum tunnelling. Moreover, transcriptomics was used, and we show that electrical-molecular communication is targeted in cancer cells. This represents a wireless electrical-molecular communication tool that facilitates cancer cell killing.

4. Acknowledgements: This work was supported by the Engineering and Physical Sciences Research Council Grant number [EP/R004072/1], Royal Society of Chemistry Enablement grant E21-1135058786, University of Nottingham internal funding schemes - NanoPrime and UNICAS. The authors would like to thank Mr Baokang Xie at Nanjing University, China for PRS and DFM analysis, David Onion at University of Nottingham, Flow cytometry Unit for assistance with flow cytometry analysis, Dr Mike Fay for help with TEM, and Jordan Potts & Ruby Brown for assistance with particle analysis.

5. Conflict of Interest: Patent Information

References:

1 McLaughlin, K. A. & Levin, M. Bioelectric signaling in regeneration: mechanisms of ionic controls of growth and form. *Developmental biology* **433**, 177-189 (2018).

2 Schofield, Z. *et al.* Bioelectrical understanding and engineering of cell biology. *Journal of the Royal Society Interface* **17**, 20200013 (2020).

3 Levin, M. Bioelectric signaling: Reprogrammable circuits underlying embryogenesis, regeneration, and cancer. *Cell* **184**, 1971-1989 (2021).

4 Lambert, N. *et al.* Quantum biology. *Nature Physics* **9**, 10-18 (2013).

5 O'Reilly, E. J. & Olaya-Castro, A. Non-classicality of the molecular vibrations assisting exciton energy transfer at room temperature. *Nature communications* **5**, 1-10 (2014).

6 Cordier, B. A., Sawaya, N. P., Guerreschi, G. G. & McWeeney, S. K. Biology and medicine in the landscape of quantum advantages. *Journal of the Royal Society Interface* **19**, 20220541 (2022).

7 Garrido, C. *et al.* Mechanisms of cytochrome c release from mitochondria. *Cell Death & Differentiation* **13**, 1423-1433 (2006).

8 Devault, D., Parkes, J. H. & Chance, B. Electron tunnelling in cytochromes. *Nature* **215**, 642-644 (1967).

9 Wuttke, D. S., Bjerrum, M. J., Winkler, J. R. & Gray, H. B. Electron-tunneling pathways in cytochrome c. *Science* **256**, 1007-1009 (1992).

10 Xin, H. *et al.* Quantum biological tunnel junction for electron transfer imaging in live cells. *Nature communications* **10**, 1-11 (2019).

11 Bordonaro, M. Quantum biology and human carcinogenesis. *Biosystems* **178**, 16-24 (2019).

12 Sanjuan-Alberte, P. *et al.* Wireless nanobioelectronics for electrical intracellular sensing. *ACS Applied Nano Materials* **2**, 6397-6408 (2019).

13 Warakulwit, C. *et al.* Dissymmetric carbon nanotubes by bipolar electrochemistry. *Nano letters* **8**, 500-504 (2008).

14 Guo, Q., Lei, C., Chen, W., Zhang, J. & Huang, B. Electric-field-driven nanoparticles produce dual-functional bipolar electrodes and nanoelectrolytic cells for water remediation. *Cell Reports Physical Science* **2**, 100299 (2021).

15 Loget, G. & Kuhn, A. Electric field-induced chemical locomotion of conducting objects. *Nature communications* **2**, 1-6 (2011).

16 Loget, G., Roche, J. & Kuhn, A. True bulk synthesis of Janus objects by bipolar electrochemistry. *Advanced materials* **24**, 5111-5116 (2012).

17 Loget, G. & Kuhn, A. Shaping and exploring the micro-and nanoworld using bipolar electrochemistry. *Analytical and Bioanalytical Chemistry* **400**, 1691-1704 (2011).

18 Robinson, A. J. *et al.* Impedimetric Characterization of Bipolar Nanoelectrodes with Cancer Cells. *ACS omega* **6**, 29495-29505 (2021).

19 Hicks, J. M. *et al.* Electric Field Induced Biomimetic Transmembrane Electron Transport Using Carbon Nanotube Porins. *Small* **17**, 2102517 (2021).

20 Brown, G. C. & Borutaite, V. Regulation of apoptosis by the redox state of cytochrome c. *Biochimica et Biophysica Acta (BBA)-Bioenergetics* **1777**, 877-881 (2008).

21 Fosdick, S. E., Knust, K. N., Scida, K. & Crooks, R. M. Bipolar electrochemistry. *Angewandte Chemie International Edition* **52**, 10438-10456 (2013).

22 Potts, J., Jain, A., Amabilino, D. B., Rawson, F. & Pérez-García, L. Molecular Surface Quantification of Multi-Functionalized Gold Nanoparticles Using UV-Vis Spectroscopy Deconvolution. (2022).

23 Chen, X., Ferrigno, R., Yang, J. & Whitesides, G. M. Redox properties of cytochrome c adsorbed on self-assembled monolayers: a probe for protein conformation and orientation. *Langmuir* **18**, 7009-7015 (2002).

24 Neumann-Spallart, M. & Kalyanasundaram, K. On the one and two-electron oxidations of water-soluble zinc porphyrins in aqueous media. *Zeitschrift für Naturforschung B* **36**, 596-600 (1981).

25 Occhiuto, I. G. *et al.* Controlling J-Aggregates formation and chirality induction through demetallation of a zinc (II) water soluble porphyrin. *International Journal of Molecular Sciences* **21**, 4001 (2020).

26 Smith, S. J. *et al.* Metabolism-based isolation of invasive glioblastoma cells with specific gene signatures and tumorigenic potential. *Neuro-oncology advances* **2**, vdaa087 (2020).

27 Jain, A. *et al.* Electric field responsive nanotransducers for glioblastoma. *Bioelectronic medicine* **8**, 1-9 (2022).

28 Kim, E. H., Song, H. S., Yoo, S. H. & Yoon, M. Tumor treating fields inhibit glioblastoma cell migration, invasion and angiogenesis. *Oncotarget* **7**, 65125 (2016).

29 Brentnall, M., Rodriguez-Menocal, L., De Guevara, R. L., Cepero, E. & Boise, L. H. Caspase-9, caspase-3 and caspase-7 have distinct roles during intrinsic apoptosis. *BMC cell biology* **14**, 1-9 (2013).

30 Brat, D. J., Bellail, A. C. & Van Meir, E. G. The role of interleukin-8 and its receptors in gliomagenesis and tumoral angiogenesis. *Neuro-oncology* **7**, 122-133 (2005).

31 Kore, R. A. *et al.* Hypoxia-derived exosomes induce putative altered pathways in biosynthesis and ion regulatory channels in glioblastoma cells. *Biochemistry and biophysics reports* **14**, 104-113 (2018).

32 Wang, Y. *et al.* MT1G serves as a tumor suppressor in hepatocellular carcinoma by interacting with p53. *Oncogenesis* **8**, 1-11 (2019).

33 Luu Hoang, K. N., Anstee, J. E. & Arnold, J. N. The diverse roles of heme oxygenase-1 in tumor progression. *Frontiers in immunology* **12**, 658315 (2021).

34 Xiong, Y. & Wang, Q. STC1 regulates glioblastoma migration and invasion via the TGF-β/SMAD4 signaling pathway. *Molecular medicine reports* **20**, 3055-3064 (2019).

35 Li, Y. *et al.* Stanniocalcin-1 augments stem-like traits of glioblastoma cells through binding and activating NOTCH1. *Cancer letters* **416**, 66-74 (2018).

36 Dong, C., Zhang, J., Fang, S. & Liu, F. IGFBP5 increases cell invasion and inhibits cell proliferation by EMT and Akt signaling pathway in Glioblastoma multiforme cells. *Cell division* **15**, 1-9 (2020).

37 Sahu, S. K. *et al.* FBXO32 promotes microenvironment underlying epithelial-mesenchymal transition via CtBP1 during tumour metastasis and brain development. *Nature communications* **8**, 1-18 (2017).

38 Zhao, J. *et al.* "Size-Independent" single-electron tunneling. *The journal of physical chemistry letters* **6**, 4986-4990 (2015).

39 De Boer, B. *et al.* Metallic contact formation for molecular electronics: interactions between vapor-deposited metals and self-assembled monolayers of conjugated mono- and dithiols. *Langmuir* **20**, 1539-1542 (2004).

40 Tang, M. L., Oh, J. H., Reichardt, A. D. & Bao, Z. Chlorination: a general route toward electron transport in organic semiconductors. *Journal of the American Chemical Society* **131**, 3733-3740 (2009).

41 Gupta, C. *et al.* Quantum tunneling currents in a nanoengineered electrochemical system. *The Journal of Physical Chemistry C* **121**, 15085-15105 (2017).

42 Kong, F.-F. *et al.* Wavelike electronic energy transfer in donor–acceptor molecular systems through quantum coherence. *Nature Nanotechnology*, 1-8 (2022).

43 Greensite, J. *An Introduction to Quantum Theory*. (IOP Publishing Bristol, 2017).

44 Choi, Y., Kang, T. & Lee, L. P. Plasmon resonance energy transfer (PRET)-based molecular imaging of cytochrome c in living cells. *Nano letters* **9**, 85-90 (2009).

45 Jing, C. *et al.* New insights into electrocatalysis based on plasmon resonance for the real-time monitoring of catalytic events on single gold nanorods. *Analytical chemistry* **86**, 5513-5518 (2014).

46 Zhou, H. *et al.* Optical monitoring of faradaic reaction using single plasmon-resonant nanorods functionalized with graphene. *Chemical Communications* **51**, 3223-3226 (2015).